Cold Regions Science and Technology 171 (2020) 102959

Contents lists available at ScienceDirect

Cold Regions Science and Technology

journal homepage: www.elsevier.com/locate/coldregions

Consolidation of fresh ice ridges for different scales

Evgenii Salganik[a,*], Knut Vilhelm Høyland[a], Sönke Maus[b]

[a] Sustainable Arctic Marine and Coastal Technology (SAMCoT), Centre for Research-based Innovations (CRI), Norwegian University of Science and Technology, Institutt for bygg- og miljøteknikk NTNU, 7491 Trondheim, Norway

[b] Department of Civil and Environmental Engineering, Norwegian University of Science and Technology, Institutt for bygg- og miljøteknikk NTNU, 7491 Trondheim, Norway

ARTICLE INFO

Keywords:
Ice ridges
Thermodynamics
Consolidation
Laboratory
Scaling

ABSTRACT

This study characterizes the refreezing process of deformed ice. Twenty laboratory experiments in ice ridge consolidation were conducted to study the influence of ridge blocks size, initial temperature, and top surface roughness on the consolidation rate. Experiments covered a ridge block thickness range of 2–6 cm, initial block temperatures from −1 °C to −23 °C, ridge sail height up to 3 cm, and consolidated layer thickness up to 14 cm. Experiments were conducted with the average value of the convectional heat transfer coefficient of 20 W/m^{2}K. The presented analytical model for ridge solidification was able to predict the observed ice growth rates and differences between level ice and consolidated layer thicknesses at different stages of the experiments. For the provided experiments, the consolidated layer was as much as 2.2–2.8 times thicker than the surrounding ice level. The consolidation rate was lower than in the analytical solution at the start of the experiment and approached the analytical solution only when the thickness of the surrounding level ice was larger than the ridge void width. The developed numerical model confirmed the observed experimental effects from the block size, initial temperature and surface roughness. Both numerical and analytical models can predict solidification rates for previous studies at the large range of scales for both fresh and saline ice. The advantages of the simplified experimental ridge geometry include high accuracy of the main parameters governing the process, including the ridge macroporosity.

1. Introduction

1.1. Motivation

Ice covers in rivers, lakes, seas and oceans deform due to action from wind and currents, resulting in ice ridges or ice accumulations. The process may not be the same in all these cases, but as long the result is a floating accumulation of broken ice it will consolidate with time depending on the physical size of the pieces. According to the definition of the WMO (1970), an ice ridge is a line or wall of broken ice that is forced up by pressure. Ridges usually consist of a sail and a keel above and below the water level, respectively. The keel initially consists of randomly packed ice blocks separated by water-filled voids described by the ridge macroporosity. Due to cooling from the atmosphere, the keels consolidate by freezing of these voids, largely proceeding vertically downwards and forming the consolidated layer (Leppäranta et al., 1995). This layer may be thicker than the surrounding level ice and constitutes a threat to the marine, coastal or hydraulic infrastructure, such as bridges, pipelines, lighthouses, range markers, fixed and floating facilities for production of oil and gas or offshore wind, harbours and ships. Ice ridges are also key features in climate studies as they constitute a large fraction of the ice volume, and because they melt more slowly than level ice. The consolidation process occurs over different timescales; ice accumulation in rivers may persist for hours or days, ridges in lakes and seas with seasonal ice cover persist a few months and the ridges in the Arctic basin and other areas with summer ice can persist a few years. Leppäranta et al. (1995), Blanchet (1998), Høyland (2002), Strub-Klein and Høyland (2011) described the seasonal development of the consolidated layer.

Høyland and Liferov (2005) distinguished among three phases of consolidation: the initial phase, the main phase and the decay phase. During the initial phase, the broken pieces of ice are submerged in the water. As they usually have lower temperatures than water at the freezing point, the temperature in the ice increases in the initial phase. The heat comes from latent heat release in the water voids and thus implies that the ice pieces grow in all directions, decreasing the macroporosity of the layer of ice pieces. Such a change is due to faster 3D diffusion than the 1D consolidation processes, justifying the separate

* Corresponding author at: Department of Civil and Environmental Engineering, Norwegian University of Science and Technology, Høgskoleringen 7a, Trondheim 7491, Norway.

E-mail addresses: evgenii.salganik@ntnu.no (E. Salganik), knut.hoyland@ntnu.no (K.V. Høyland), sonke.maus@ntnu.no (S. Maus).

https://doi.org/10.1016/j.coldregions.2019.102959
Received 23 August 2019; Received in revised form 6 November 2019; Accepted 2 December 2019
Available online 04 December 2019

treatment of this phase. During the main phase, consolidation of this layer takes place largely one-dimensionally from top to bottom, before it starts to melt in the decay phase. Ice ridges that do not survive a summer melt are called first-year ice ridges, and the available field data on ridge morphology have been summarized by Strub-Klein and Sudom (2012).

Physical parameters of broken ice features can be studied in the field, but these investigations are time-consuming and are usually unable to provide data about the ridge formation process, initial conditions before consolidation, and potential full-scale loads on offshore structures and vessels. Thus, many of the parameters governing consolidation process are unknown or quite uncertain: initial macroporosity (liquid water content), initial size, orientation, salinity and temperature of broken ice blocks forming the ridge, and thickness of the snow above the ridge.

Predicting the thickness of the consolidated layer for these different timescales is important, and in an engineering context, scale-model testing is often conducted for this purpose. In such tests, the physical size of the problem is significantly reduced with a geometric scale factor, and the other relevant factors and processes must be scaled in such a way that the correct full-scale ice forces can be predicted (Langhaar, 1951; Palmer and Dempsey, 2009). Thus, the consolidation process should be understood not only for different timescales but also for different sizes, leading to several unsolved challenges (Høyland, 2007, Repetto-Llamazares, 2010; Høyland, 2010). Previous consolidation models did not include scale effects (Leppäranta, 1993), while in laboratory experiments (Timco and Goodrich, 1988; Blanchet, 1998) and field experiments (Leppäranta et al., 1995; Høyland, 2002), such effects were observed. However, laboratory-scale models of ice ridges also involve scaling of ice mechanical properties using dopants, which complicates the solidification process because the temperature-dependent liquid fraction and microstructure of the model ice differ from the field.

There are important differences between fresh ice and saline ice thermodynamics. However, with respect to ice growth rates, the differences are small. The numerical model of Maykut and Untersteiner (1969) provided a 7% higher equilibrium ice thickness for fresh ice. Notz (2005) presented experimental results for saline ice growth, showing that the growth rate of saline ice cooled from above is close to that of fresh ice (in contrast to saline ice cooled in a non-natural way from below due to the absence of the ice desalinization process). Petrich et al. (2007) presented both analytical and experimental analyses of the ice-opening refreezing process, showing that his model describes this process for both seawater and freshwater assuming different values of latent heat and ice thermal conductivity for both types of ice. Griewank and Notz (2013) showed that different salinity profiles could change ice thickness predictions by less than 4%. For ridges, Timco and Goodrich (1988) found no difference between level ice and ridge consolidation for fresh water and EG/AD/S water solution, and for the full scale, the ratios of the consolidated layer and surrounding level ice in almost fresh Baltic ridges compared well with those observed in saline ridges (Høyland, 2002). The physical basis for the similar growth rates for fresh and saline ice is that its growth rate is proportional to the value of the square route of thermal conductivity divided by the density and latent heat (Stefan, 1891; Leppäranta and Hakala, 1992; Petrich et al., 2007). The difference in this value between sea ice and fresh ice at the water freezing temperature is less than 4% (Schwerdtfeger, 1963; Yen, 1981; Notz, 2005).

Our research goal is to study ice ridge consolidation on laboratory scales to improve understanding of ridge thermodynamics in general. To exclude complications due to microstructure and solute rejection, we study freshwater ice and focus on ridge consolidation and macroporosity. Small-scale experiments are performed and the results compared to those from a one-dimensional analytical model and a two-dimensional numerical model. The results are interpreted in terms of their upscaling potential to larger scales.

1.2. Previous studies

The growth rate of the consolidated layer in time t is a function of the meteorological conditions (air and water freezing temperatures T_a and T_w, wind speed, long and shortwave radiation and snow thickness), the actual ice thickness and the ridge macroporosity. The oceanic flux becomes important in the decay phase but has little effect in the main phase. An easy way to allow for comparison between different temporal and physical scales is to perform a comparison with the surrounding level ice thickness. Leppäranta and Hakala (1992) assumed that level ice has the same surface flux and that the only difference is the ridge macroporosity η, and they defined a non-dimensional factor R by dividing the thickness of the consolidated layer h_c with the surrounding level ice thickness h_i:

$$R = h_c/h_i = \eta^{-0.5} \quad (1)$$

Most ridge growth models, including the international standard (ISO 19906, 2010), use this approach. The level ice surrounding a ridge can be of different origins. It may be (a) level ice from which the ridge has formed and that has continued to grow since that time, or it may be (b) level ice that started forming in a lead created by ridge formation (Fig. 1). The former will be thicker than the latter, and the ratio R and its history will differ for the cases. In case (a), R will start at a value lower than equilibrium, while in case (b), it will approach equilibrium from above. Although it is often different to determine this origin in the field, it is known in the laboratory, allowing a more concise analysis and model evaluation.

Only a couple of field studies and even fewer laboratory investigations on the growth of the consolidated layer have been conducted. Both fresh and doped ice have been used in laboratories, and both saline and Baltic ridges have been monitored in situ. Independent of the ice type, the ratio of the consolidated layer to level ice thicknesses R seems to approach a similar asymptotic value for both small-scale and full-scale measurements. The laboratory investigations provided a higher R values with a decreasing trend, whereas the trend was increasing in situ (Fig. 2).

The basin experiments (Timco and Goodrich, 1988) showed a

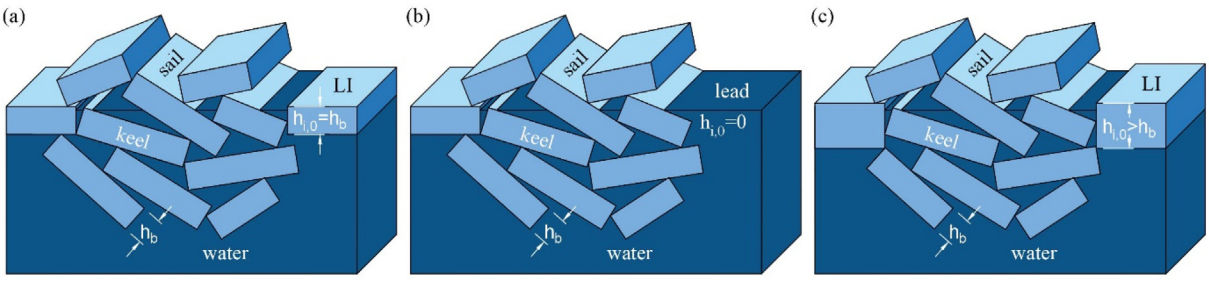

Fig. 1. Scheme of an ice ridge formed from uniform level ice with thickness $h_{i,0} = h_b$ (a), formed close to a newly formed lead with zero ice thickness $h_{i,0} = 0$ (b), and formed from closure of a lead by a thicker level ice $h_{i,0} > h_b$ (c).

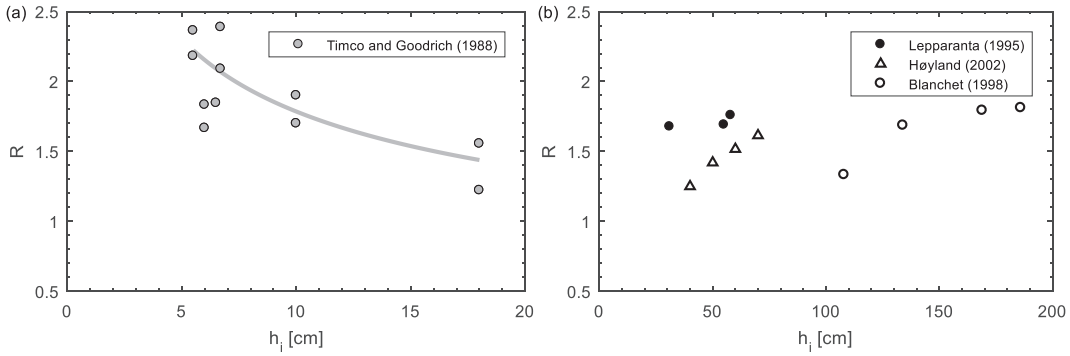

Fig. 2. The ratio of the consolidated layer to level ice thicknesses R vs level ice thickness h_i from laboratory experiments by Timco and Goodrich (1988) (a) and from field data by Leppäranta et al. (1995), Høyland (2002) and Blanchet (1998) (b).

decreasing trend and larger R values for a lower level ice thickness (Fig. 2a). The consolidation layer thickness in their experiments was in the range from 10 to 28 cm; the level ice was 5–18 cm. Ridge macroporosity was not measured, ice was both fresh and model (EG/AD/S), and wind speed was 0.2 cm/s, but the effect of additional growth from a higher local wind speed was measured. Field experiments are difficult to compare with analytical solutions due to uncertainty in the ice initial thickness. Leppäranta et al. (1995) showed increasing R values during their field experiment with an initial level ice thickness of 0.31 m and macroporosity of 0.28. Blanchet (1998) presented fieldwork results with the same increasing trend and initial level ice thickness of 0.83 m. Høyland (2002) showed increasing time R values for ridges in Svalbard and in the Baltic Sea (Fig. 2b).

Measurements of the consolidated layer are more difficult than for level ice. Three methods are mainly used: mechanical drilling, thermal drilling and analysis of vertical temperature profiles. Results using the drilling method can provide higher values than temperature profiles (Høyland, 2002). Kharitonov (2008) used the thermal drilling method and found average consolidated layer thickness values equal to 0.83–1.63 of the level ice thickness for ridges with an average keel macroporosity ranging from 0.12–0.28. Kharitonov and Morev (2009) presented an analysis of the sail height effect on ridge consolidation. Wazney et al. (2019) performed small-scale mechanical experiments with fresh deformed ice, showing that the consolidation time was the key factor for the maximum loads.

Since level ice thickness is commonly used to define the R value as in Eq. (1), it is important to provide an overview of its growth models and their scalability. The first analytical model was published by Stefan (1891) and includes only conduction and latent heat fluxes under the assumption of an ice top surface temperature equal to the air ambient temperature. To obtain accurate results with this model, ice temperatures should be accurately measured. Adams et al. (1960) added sensible heat, air convection and wind speed effect to the growth model, which made it possible to predict thin ice growth in an accurate manner. Maykut and Untersteiner (1971) presented a one-dimensional model of sea ice growth, including incoming and outgoing longwave and shortwave radiation, conduction in snow and ice, convection in water, and sensible heat. Ashton (1989) analysed the effects of wind speed on air convection and thin ice growth and compared them with field experiments. Leppäranta et al. (1995) presented a summary of analytical ice growth models. Notz (2005) conducted a detailed review of sea ice thermodynamic parameters and experiments examining sea ice desalinization.

To perform experiments evaluating small-scale ridge consolidation, it is important to analyse existing setups of basin tests to obtain useful data. According to Repetto-Llamazares (2010), key parameters of the average model first-year ridge include a keel depth of 30 cm, sail height of 7 cm, blocks of 10 × 8 × 3 cm, a porosity of 20–40%, and level ice thickness of 6 cm. For full-scale ridges, the average ratio of keel to sail heights k/s is 5.2, the average relation of sail height and block thickness is $s \cong 3.73\sqrt{w}$, the average sail height s is 2 m (Strub-Klein and Sudom, 2012), and the unconsolidated keel macroporosity also ranges from 20 to 40% (Høyland, 2007; Pavlov et al., 2016; Bonath et al., 2018).

The consolidation problem has similarities with the formation of refrozen cracks in ice, which have been described and modelled by Petrich et al. (2007). Their model has boundary conditions assuming a linear temperature profile in the surrounding ice at a certain distance. For the consolidation problem, this assumption would require one layer of horizontal blocks with a ratio of block length and thickness larger than two, which cannot be treated as the ice ridge.

2. Analytical model

2.1. Governing equations

The consolidation rate of fresh ice ridges in a laboratory is mainly governed by air temperature, wind speed, and ridge configuration. In the field, it is also affected by oceanic fluxes from the bottom, long and shortwave radiation, and presence of snow. The ridge is a porous medium consisting of ice and water. In contrast to level ice growth, its solidification cannot be accurately modelled as a one-dimensional problem without significant simplifications. Nevertheless, under the assumption of homogeneity, this problem can be solved in a single dimension, which literally means that the homogeneous ridge consists of a mixture of infinitely small ice blocks surrounded by water. The consolidated layer thickness and initial block size are on the same order for short consolidation times.

Ice growth includes heat transfer from the water via conduction through the ice into convective heat transfer in the air. The amount of newly formed ice h_i depends on the sum of the conductive heat flux q_c and the heat flux from the water q_w. It can be expressed as

$$-\rho_i L_i \partial h_i/\partial t = q_c + q_w, \tag{2}$$

where ρ_i is the ice density, L_i is the ice latent heat, and t is the time.

The oceanic heat flux q_w is an external energy source. It can be determined from an oceanic model and will be assumed to be zero for laboratory conditions. The conductive heat flux q_c depends on the ice bottom and top surface temperatures T_f and T_s, and its thickness h_i according to Fourier's law:

$$q_c = -k_i \partial T/\partial z \cong k_i (T_f - T_s)/h_i, \tag{3}$$

where k_i is the ice thermal conductivity. This equation neglects internal heat storage related to the specific heat needed to cool the ice and assumes a constant thermal conductivity.

The heat flux from the ice or snow surface into the air consists of the turbulent heat exchange with the atmosphere and the radiation balance. It depends on the atmospheric conditions, characteristics of the surface type, and surface temperature of the ice/snow system. For thin

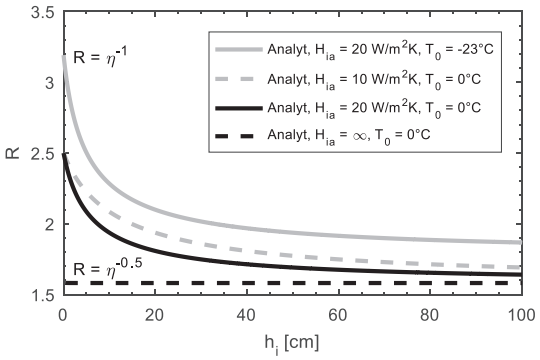

Fig. 3. Ratio of consolidated layer and level ice thicknesses $R = h_c/h_i$ vs level ice thickness h_i for the analytical solution from Eqs. (6), (8) and (9) and initial macroporosity η_0 of 0.4 for the different initial block temperatures T_0 and heat transfer coefficient H_{ia}.

ice, the turbulent heat flux is dominating (Adams et al., 1960). The convectional heat transfer is then expressed as a linear function of the temperature difference between the ice surface and the atmosphere (Newton's law of cooling):

$$q_a = H_{ia}(T_s - T_a), \tag{4}$$

where H_{ia} is the convectional heat transfer coefficient.

Assuming an insignificant effect from long and shortwave radiation, and the absence of snow, one can set $q_c = q_a$ to obtain the ice top surface temperature T_s. Setting Eq. (5) in Eq. (3), one can then integrate Eq. (2) to obtain the ice thickness h_i, Eq. (6):

$$T_s = \frac{k_i T_f + H_{ia} h_i T_a}{k_i + H_{ia} h_i}; \tag{5}$$

$$h_i = \left(\frac{2k_i}{\rho_i L_i}(T_f - T_a)t + \left(\frac{k_i}{H_{ia}}\right)^2\right)^{0.5} - \frac{k_i}{H_{ia}} \tag{6}$$

In all previous publications and engineering standards, ice ridges are implicitly assumed as a homogeneous media with small pores that are evenly distributed in its volume. For such a ridge, we can assume that we have to freeze only the liquid fraction η inside the ridge volume (Leppäranta, 1993):

$$L_c = L_i \eta \tag{7}$$

Inserting this in Eq. (6), we can obtain consolidated layer thickness analytical solution for homogeneity assumption:

$$h_c = \left(\frac{2k_i}{\rho_i L_i \eta}(T_f - T_a)t + \left(\frac{k_i}{H_{ia}}\right)^2\right)^{0.5} - \frac{k_i}{H_{ia}} \tag{8}$$

The initial phase of ridge consolidation can be included in the described analytical model by assuming a change in initial porosity from η_0 to η, where η_0 is the porosity prior to the temperature change from the initial ice temperature T_0 to the water temperature T_f:

$$\eta = \eta_0 - (1 - \eta_0)\frac{c_i(T_f - T_0)}{L_i} \tag{9}$$

This implies a relative additional ice volume $\eta - \eta_0$ be formed after the end of the initial phase of ridge consolidation. How fast is this initial change in comparison to vertical ice growth? The duration of the initial phase depends on the initial temperature T_0 and characteristic block thickness w according to the solution of the heat diffusion equation in the x-axis direction of the smallest block dimension:

$$c_i \rho_i \frac{\partial T}{\partial t} = \frac{\partial T}{\partial x}\left(k_i \frac{\partial T}{\partial x}\right) \tag{10}$$

The approximate form of the solution for the initial temperature T_0 and $t \geq 1/\pi^2$ is

$$T(x,t) \approx \frac{4T_0}{\pi} sin(\pi x) e^{-\pi^2 t} \tag{11}$$

This is a dimensionless solution, which means that dimensional time t′ can be expressed as

$$t' = \frac{c_i \rho_i w^2 t}{k_i} \tag{12}$$

The temperature at the centre of the block at time $t = 1/\pi^2$ is only 47% of the initial temperature T_0. We can assume the thermal equilibrium conditions after the initial phase when we are within 1% of the freezing point $T_{eq} = T_f - 0.01(T_f - T_0)$. For example, the equilibrium time t_{eq} for 4-cm-thick blocks is only 12 min, which means that we can assume that ice growth during the initial phase can occur immediately after the start of an experiment for the analytical model of ridge solidification.

The simplifications expressed in Eqs. (7)–(9) provide a one-dimensional solution of the consolidation problem based on the amount of freezing degree-days and the macroporosity η. We use this model to investigate the effect of the convectional heat transfer coefficient H_{ia}, introduced in Eq. (4), on the ratio R. The model shows that assuming an ice surface temperature equal to the air temperature ($H_{ia} = \infty$) significantly underestimates the R values for a level ice thickness less than 20–30 cm. In reality, the ice top surface temperature is a function of the ice thickness as well as the heat flux into the air. Accounting for this effect of finite heat transfer coefficient demonstrates a significant scale effect of the consolidated layer and level ice growth rate ratio (Fig. 3): the R value starts at η^{-1} and only approaches $\eta^{-0.5}$ for thick ice.

The convectional heat transfer coefficient H_{ia} for steady laboratory conditions can be back-calculated using Eq. (5) from the experimental level ice thickness for the corresponding temperatures:

$$H_{ia} = \frac{k_i(T_f - T_s)}{h_i(T_s - T_a)} \tag{13}$$

In summary, the R value is a function of several variables: the initial macroporosity η_0, the level ice thickness h_i, the initial ice temperature T_0, and the convectional air-ice heat transfer coefficient H_{ia}.

It is possible to normalize R with respect to some of these variables. The macroporosity may not be the same in all data, so an easy approach is to divide by the equilibrium value ${\eta_0}^{-0.5}$, which will only be correct with the infinite heat transfer coefficient H_{ia}, zero thermal inertia $c_p \Delta T$, and infinitely small block size w. In this case, the equilibrium value of $R{\eta_0}^{0.5}$ becomes one. The number of accumulated freezing degree-days $(T_f - T_a)t$ is assumed to be the same for both level ice and the consolidated layer. We may use Eqs. (6) and (8), and introduce a normalized solution, allowing for comparison between experiments with a different convective heat transfer coefficient (H_{ia}), macroporosity (η_0) and ice thickness (h_i):

$$R_{norm} = \left(\frac{h_c(h_c + 2k_i/H_{ia})}{h_i(h_i + 2k_i/H_{ia})}\eta_0\right)^{0.5} \tag{14}$$

This factor has the same dimension of [m/m] as the R value but reduces the experimental variance. The analytical solution for this factor provides a value of 1 for any macroporosity, allowing separate investigations of other factors influencing consolidation. Eq. (9) was used to account for the ice initial temperature of −23 °C, giving an R_{norm} value of 1.13. The value of the initial macroporosity η_0 was used for normalisation to experimentally and numerically assess the validity of Eq. (9) and the effect of the initial block temperature T_0 on the freezing rates.

The main geometric parameters of the model ridge are defined in Fig. 4b. Other factors influencing the values of R, including the sail height s, block thickness w and keel depth k, are not included in the analytical model and are not normalized. Their effect will be described in Section 4 based on the experimental and numerical results.

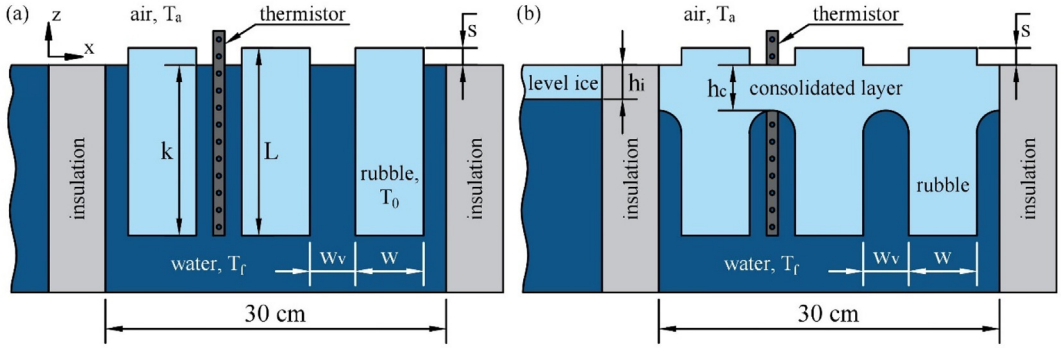

Fig. 4. Scheme of the experimental setup at the start (a) and end (b) of the experiment.

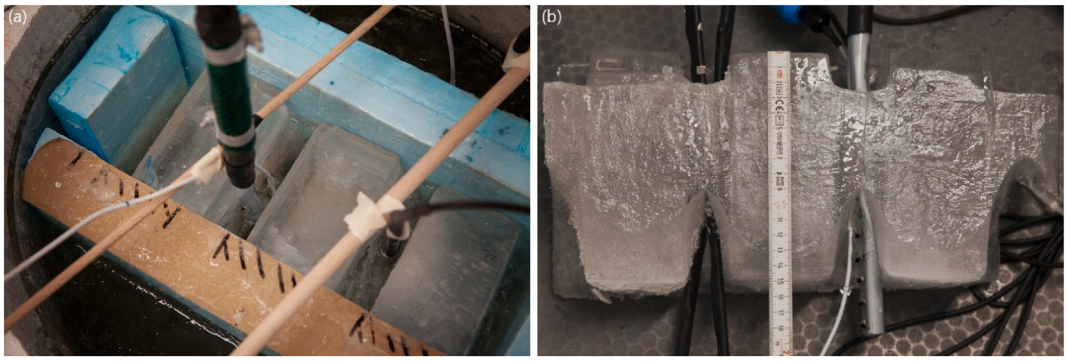

Fig. 5. Experimental setup before (a) and after (b) consolidation.

2.2. Ice growth and thermodynamics

For comparison with observations, it is useful to consider the simplifications made in the analytical model, which are as follows: neglecting specific heat and temperature dependencies (e.g., the thermal conductivity of ice); and a constant heat transfer coefficient H_{ia}. For fresh ice, most of the thermodynamic parameters are slightly temperature-dependant at atmospheric pressure. According to Pounder (1965), the density of pure ice depends slightly on temperature as follows:

$$\rho_i = 916.8 - 0.1403 \cdot T \quad (15)$$

According to Yen et al. (1991), pure ice thermal conductivity is

$$k_i = 2.21 - 1.00 \cdot 10^{-2} T + 3.44 \cdot 10^{-5} T^2 \quad (16)$$

Pure ice heat capacity from Weast (1971) can be determined as

$$c_i = 2112.2 + 7.6973 \cdot T \quad (17)$$

The latent heat of fusion L_i of water is 333.5 kJ/kg, according to Feistel and Hagen (1998). For analytical solutions, it is sufficiently accurate to use values at 0 °C corresponding to the bottom surface of the ice slab. For a temperature range between 0 °C and − 20 °C, the thermal conductivity typically changes by 1%.

As an example, we performed a comparison of the analytical solution with constant thermodynamic parameters and provided a numerical solution with temperature-dependent values of ρ_i, k_i and c_i for level ice growth with an ambient air temperature of −15 °C and heat transfer coefficient of 20 W/m^{2}K over 1000 h. The difference in final ice thickness was 1.2%. For small-scale experiments, this difference was even smaller because ice is significantly warmer. Using the simple Stefan equation, the difference in $(k_i/\rho_i L_i)^{0.5}$ was only 3.4% larger for −15 °C than for 0 °C. The difference between analytical and numerical results with constant values of ρ_i, k_i and c_i was less than 0.3%.

The heat transfer coefficient H_{ia} may vary with temperature, wind conditions, stratification and surface roughness. Practically, it has been found to vary from approximately 10 W/m^{2}K for still air to 30 W/m^{2}K for windy conditions (e.g., Ashton, 1989). In comparison to thermodynamic properties, the heat transfer coefficient dominates the uncertainty in simulations of thin ice growth.

3. Experiments

3.1. Experimental methods

Twenty tests were conducted to study the influence of the rubble block size, orientation and initial temperature on the consolidation rate. Fresh ice was cut into pieces, cooled down to the chosen temperature T_0, placed in the water tank with side thermal insulation, and frozen under laboratory conditions with an air temperature T_a of −15 °C (Fig. 4). Ice blocks were vertical or inclined by 30° from the water surface. The thickness of the ice blocks w was 2, 4 or 6 cm; the length L was 15 cm, and the depth was 10 cm through all experiments. The initial thickness for both level ice and the consolidated layer was zero (see Fig. 4b for the definition). The initial water temperature was 0 °C, and the initial ice block temperature was −1, −15 or −24 °C. The size of the side insulation box was 25 × 30 × 10 cm (Fig. 5a). The top surface roughness was characterized by the sail height s, which varied for different tests in the range from 0 to 3 cm. The keel depth value k was equal to the difference between block length L and sail height s. One longer thermistor string (100 cm long with 3 cm sensor spacing) was installed to measure air temperature, one identic thermistor together with a shorter thermistor (15 cm long with 1.5 cm spacing) were installed to measure ice and water temperatures. The initial macroporosity η_0 in the range from 0.32–0.43 was calculated as $w_v/(w + w_v)$, and values of the block and void width w and w_v were obtained from photo images taken before the consolidation. Both level ice and consolidated layer thicknesses were measured directly after each experiment. Additionally, the level ice thickness was measured during the experiment by drilling. The consolidated layer thickness was measured by drilling only in six tests to avoid ice volume disturbances.

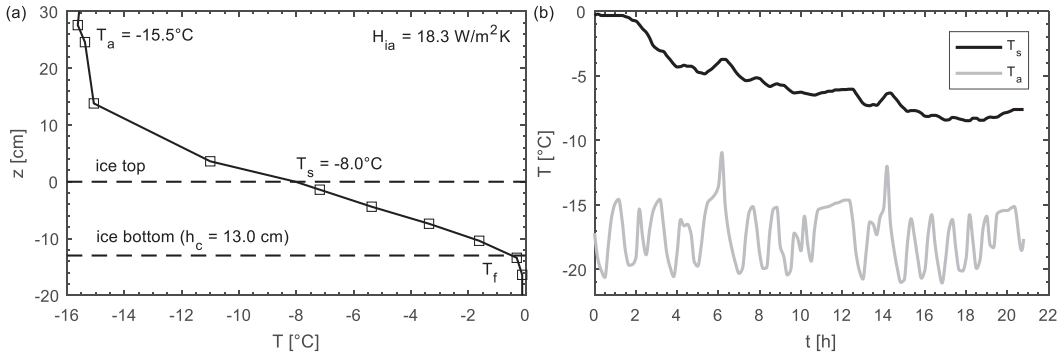

Fig. 6. Temperature vs depth after 20 h of the consolidation experiment 16 (a) and the air and consolidated layer top surface temperature vs time for experiment 16 (b).

Ridge consolidation is mainly governed by thermodynamics, and most of the information can be retrieved from thermistor strings. The temperature profile in the air above the ice was non-linear in the range of the boundary layer (Fig. 6a), and the thickness of this layer depended on the ice thickness. The boundary layer reached 15 cm in our experiments. The ice surface temperature depended on the ratio between conduction in the ice and convection in the air, so it could be estimated from the temperature gradient in ice and convectional heat transfer coefficient H_{ia} depending mainly on the air velocity (Fig. 6a). The consolidated layer thickness h_c in this paper was assumed to be the minimum thickness of newly formed ice after the ridging process (Fig. 4b).

The final thicknesses, air and ice temperatures were measured directly in the experiments. Ice top surface temperature was derived using temperature profiles with a certain accuracy depending on the sensor precision and spacing. In this paper, the following method was used: all sensors with a temperature below -0.3 °C were assumed to be within the ice. For these sensors, the average temperature gradient was calculated. It was then extrapolated at the top and bottom sensors to determine the surface temperature at $z = 0$.

The time-averaged convectional heat transfer coefficient can be obtained from the level ice thickness development using the analytical model from Eq. (6) (Fig. 7a). It can also be obtained from air, ice top and bottom surface temperatures (Eq. (13)). This parameter cannot be completely constant in the laboratory due to the cyclic work of cooling fans – thus, time averaging might be used. The duration of the full cycle of cooling and warming for the NTNU laboratory was 40 min (Fig. 8b).

3.2. Experimental results

The summary of the performed experiments is presented in Table 1, including the main initial parameters: ice block initial temperature T_0, ridge initial macroporosity η_0, block width w, sail height s, number of accumulated freezing degree-days FDD, and block inclination α; and the final values of level ice and consolidated layer thickness h_i and h_c, their ratio R, and factor R_{norm}.

An example of the vertical temperature profile is shown in Fig. 6a together with the measured consolidated layer thickness h_c, estimated air-ice interface temperature T_s and heat transfer coefficient H_{ia}. The temporal development of the air and ice top surface temperatures T_a and T_s during a single experiment is shown in Fig. 6b.

3.2.1. Level ice growth

It is quite common that experiments focused on level ice growth provide results that deviate from theoretical predictions when plotted against FDD or $\int (T_f - T_a)dt$. A significant number of tests should be performed to obtain accurate values of the time-averaged convectional heat transfer coefficient H_{ia}. It was estimated as 20 W/m^{2}K in our laboratory (Fig. 7a). Sources of error include an uneven ice thickness, non-constant convection intensity due to cycles of cooling, and extraction of sensible heat during heating at the end of an experiment. The last effect can be clearly seen in Fig. 7a: final experimental values were larger than intermediate ones. The usage of FDD for experimental comparison results in an increasing error and is more practical to avoid the conversion from level ice thickness to FDD and back to the consolidated layer thickness (Fig. 7b).

Based on our observations, we can estimate the heat flux related to ice growth in three ways: via $q_a = H_{ia}(T_s - T_a)$ by assuming a constant H_{ia} and measured air and ice surface temperature; from $q_c = -k_i \partial T/\partial z$ based on the temperature gradient in the ice; and from $q_l = -\rho_i L_i \partial h_i/\partial t$ based on the ice growth rate. Accurate estimates of the convective q_a, conductive q_c, and latent heat fluxes q_l are clearly difficult when the ice thickness is small (Fig. 8a) due to the following factors: one needs to have two frozen sensors to properly obtain temperature gradients; the

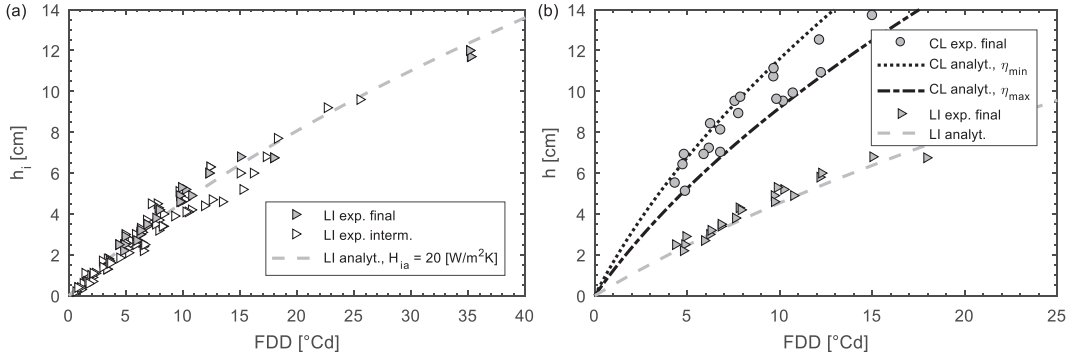

Fig. 7. Level ice thickness h_i (a) and thickness of level ice and the consolidated layer h (b) vs freezing-degree days FDD from experiments and from the analytical model for minimum and maximum experimental ridge porosities η_{min} and η_{max}.

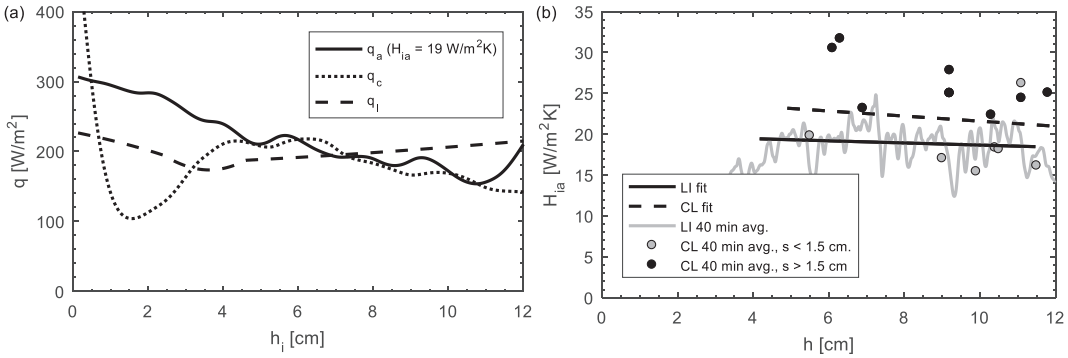

Fig. 8. Convective, conductive and latent heat fluxes q from temperature and thickness measurements vs the level ice thickness h_i (a) and heat transfer coefficient H_{ia} from temperature and thickness measurements using Eq. (13) vs the ice thickness h for the chosen level ice experiment level and for all instrumented ridge experiments (b).

assumption of linear temperature gradients may be inaccurate; ice thickness measurements from drilling are limited to an accuracy of a few mm; the heat transfer coefficient H_{ia} may not be constant over short times with relatively large temperature changes, and it may depend on the cold room cooling system.

The convectional heat transfer coefficient was estimated using Eq. (3) continuously for a single level ice experiment and for the last 40 min of each consolidation experiment due to the uncertainty of the consolidated layer thickness development (Fig. 8b). Higher values of the heat transfer coefficient H_{ia} for the consolidated layer were mostly observed when the sail height was greater than 1.5 cm. Small-scale sails added additional top surfaces for model ridges with increasing vertical heat fluxes. Several factors can change the consolidation rate, including the sail height and block thickness. Separate effects from each parameter are described in the numerical modelling results section of this paper. The level ice thickness was found to be the most accurate data for estimating the value of the convectional heat transfer coefficient (Fig. 7a).

3.2.2. Consolidation

The analytical solution from Eq. (8) significantly overestimated the R values when the level ice thickness h_i was less than the distance between blocks w_v (1.4–4.4 cm), as shown in Fig. 9a. This phenomenon will be analysed and explained using our numerical model (see Section 4). The figure further shows the effect of the initial ice temperature: colder ice consolidated faster and reached a higher maximum value. The analytical solution can be modified with Eq. (9) so that the effect of the initial temperatures is included, and the maximum values clearly correlate with the initial temperatures. Most maximum values fit in between the analytical solutions for cold and warm ice (Fig. 9b). The initial macroporosity also varied in the experiments (0.32–0.43), and most of the data fit in between these analytical solutions (Fig. 9a). Usage of R_{norm} allowed the comparison of experiments with different porosities and permitted the possibility of investigating the effects of other governing parameters. Finally, we might observe a trend of a lower value than the modelled R towards the end of the experiments, which is proposed to be an effect of the limited keel depth and will also be analysed and explained using the numerical model in Section 4.

The effect of these three parameters: sail, keel and block size – can be included only in a 2D model and will be analysed with the numerical model in Section 4. The effect of block orientation was similar to that from block thickness: the void size was higher for a higher block inclination from the vertical axis for the same block thickness. Simultaneously, experiments with inclined blocks showed a much more complicated geometry and less possibility for accurate thickness measurements. Consolidation experiments with vertical blocks of diffident thickness were found to be more convenient for scale-effect investigations.

3.3. Error sources

The described experiments include length measurements of ice

Table 1
Summary of experiments.

№	T_0 [°C]	η_0	w [cm]	s [cm]	FDD [°Cd]	α [°]	h_i [cm]	h_c [cm]	R	R_{norm}
1	−1	0.37	6.3	1.1	6.8	0	3.5	7.0	2.00	0.91
2	−1	0.36	4.6	0.0	10.7	0	4.9	9.9	2.02	0.91
3	−1	0.41	6.0	0.0	7.4	0	5.5	10.4	1.89	0.93
4	−5	0.32	6.0	0.6	12.2	0	5.8	12.5	2.16	0.97
5	−1	0.40	4.2	2.0	4.4	29	2.5	5.5	2.20	0.98
6	−1	0.40	4.8	1.7	6.8	30	3.4	8.1	2.38	1.03
7	−1	0.37	4.1	2.2	5.9	0	2.7	6.9	2.56	1.05
8	−15	0.37	4.4	0.5	4.9	39	2.9	5.1	1.76	0.84
9	−18	0.39	6.3	0.0	7.9	0	5.8	9.7	1.67	0.86
10	−15	0.33	6.0	0.0	12.3	0	6.3	11.5	1.83	0.89
11	−16	0.41	4.3	2.1	12.3	25	6.0	10.9	1.82	0.95
12	−23	0.43	4.1	0.5	10.2	0	5.2	9.5	1.83	0.99
13	−23	0.40	3.9	0.0	9.7	0	4.9	10.7	2.18	1.04
14	−23	0.35	4.2	0.5	6.3	0	3.2	8.4	2.63	1.05
15	−23	0.36	2.3	0.7	9.7	0	4.6	11.1	2.41	1.07
16	−23	0.37	4.3	2.5	15.0	26	6.8	13.7	2.01	0.97
17	−23	0.38	6.5	1.7	7.9	0	4.2	9.7	2.31	1.00
18	−23	0.43	5.7	2.4	6.2	24	3.0	7.2	2.40	1.07
19	−23	0.36	6.4	2.6	4.9	0	2.5	6.9	2.76	1.09
20	−23	0.42	4.2	2.9	7.6	0	3.8	9.5	2.50	1.10

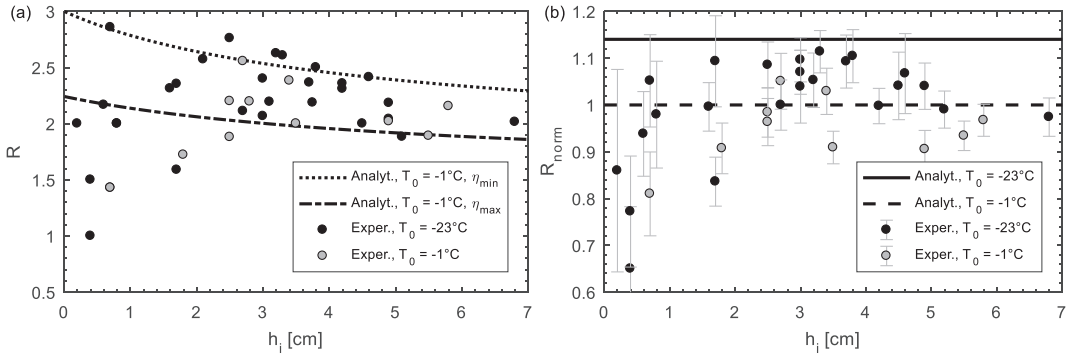

Fig. 9. Experimental results presented via R values (a) and via R_{norm} values (b) plotted against the level ice thickness h_i together with the analytical solution for the range of porosities (a) and for the range of initial block temperatures (b).

thickness, block width and sail height, leading to instrumental random error of direct and indirect measurements, which is presented using standard error bars. The known source of systematic error is the porosity irregularity when the porosity of the exact ridge void and surrounding blocks is different from the porosity of the surrounding voids. The described systematic error can be eliminated using a numerical simulation with a row of four blocks and three voids with different porosities for the central section. The local porosity is defined as the ratio of the void width and the sum of the void and half of the width of the surrounding blocks. The consolidation rate is defined by the local porosity during the initial phase. It approaches the consolidation rates for the average porosity. In the range of studied level ice thicknesses, the 10% difference in surrounding porosity results in a 5–9% difference in consolidated layer thickness in contrast to the 15–20% difference for the same change in local porosity. Another source of systematic error in porosity measurements is the presence of the thermistor with a cross-section of 1.5 cm^2 in one of the ridge voids (Fig. 5). It was accounted for by correcting the macroporosity for the thermistor cross-section.

4. Numerical simulations

Mathematical models of the solidification process can be divided into two main groups: the fixed domain and the front tracking method (Liu and Chao, 2006). The commonly used method for the first group is the effective specific heat method, which includes the latent heat in the temperature-dependent-specific heat values. This method is not very accurate when the Stefan number Ste, defined as $c/\Delta TL_i$, is small and when the two phases are in thermal equilibrium. The front tracking method was chosen for analysis in our experiments. For this method, two phases are solved separately and linked by the Stefan condition at the interface. The effective specific heat method is also applicable to the current problem. However, it requires a low temperature interval between phases, fine mesh, low relative errors, and a large computational time.

4.1. Governing equations and boundary conditions

The ridge consolidation process was modelled using the finite element analysis simulation software COMSOL Multiphysics 5.3a. Two materials were used: water and ice. Heat transfer in fluid and laminar flow packages were coupled for water simulation. The position of the ice-water boundary was defined by the Stefan energy balance condition (Eq. (19), where the difference in heat fluxes in two materials is equal to the amount of new solid formed or melted (Alexiades et al., 2003).

This numerical model requires the following material parameters for ice and water: thermal conductivity, heat capacity, density, coefficient of thermal expansion, latent heat of fusion and kinematic viscosity. Fresh ice thermodynamic parameter values are described in chapter 2.2. Other values were obtained using the Gibbs SeaWater Oceanographic Toolbox of TEOS−10 (Millero, 2010). Thermal boundary conditions were defined as thermal insulation at the sides and at the bottom, and as external convection with a constant heat transfer coefficient H_{ia} at the top (air-ice interface). The value of $H_{ia} = 20 W/m^2K$ was used based on the experimental level ice growth rate under the laboratory conditions. The heat transfer coefficient was assumed to be equal for level ice and consolidated layer growth. The air ambient temperature was equal to the mean experimental value of −15 °C.

The heat flux balance at the air-ice interface is described as follows:

$$H_{ia}(T_a - T_s) = k_i\left(\frac{\partial^2 T}{\partial x^2} + \frac{\partial^2 T}{\partial z^2}\right) \tag{18}$$

The heat flux balance at the ice-water interface is

$$\rho_i L_i v_n = k_i \frac{\partial T}{\partial n} - q_w, \tag{19}$$

where v_n is normal velocity of the ice-water interface, $\partial T/\partial n$ is normal derivative of the ice temperature at the interface.

Heat diffusion within the ice is described by

$$\rho_i c_i \frac{\partial T}{\partial t} = k_i\left(\frac{\partial^2 T}{\partial x^2} + \frac{\partial^2 T}{\partial z^2}\right) \tag{20}$$

Simulations of the ridge consolidation were performed to study the effect of the initial block temperature, block width and length, sail height, and porosity on ice growth. The numerical model setup was similar to the experimental setup shown in Fig. 4, except for the presence of a thin initial ice thickness of 1 mm at the air-water interface.

4.2. Comparison with the experimental and analytical results

The described numerical model is compared to experimental results and the analytical model in Figs. 10 and 11. In the following section, we discuss its capability to predict the observed development of the R value and the effects of the initial temperature T_0, block thickness w, sail height s, and keel depth k.

4.2.1. Block thickness effect

The 1D analytical solution deviated from observations, which was the most prominent at the beginning of the experiments. Running the 2D numerical model with different block thicknesses indicated that this deviation was a consequence of the variable block thicknesses, a 2D effect that was well-captured by the numerical model (Fig. 10a). The R_{norm} values approached equilibrium faster for thinner blocks. The figure indicates a peak in R_{norm} that was reached when level ice had grown to approximately the size of the pores (1.3 cm for 2-cm-thick blocks and 2.7 cm for 4-cm-thick blocks). Fig. 10b shows that the numerical model captured an important effect, in which for small block sizes, the R value increased, reached a maximum value and decreased. When the block size increased, this effect disappeared.

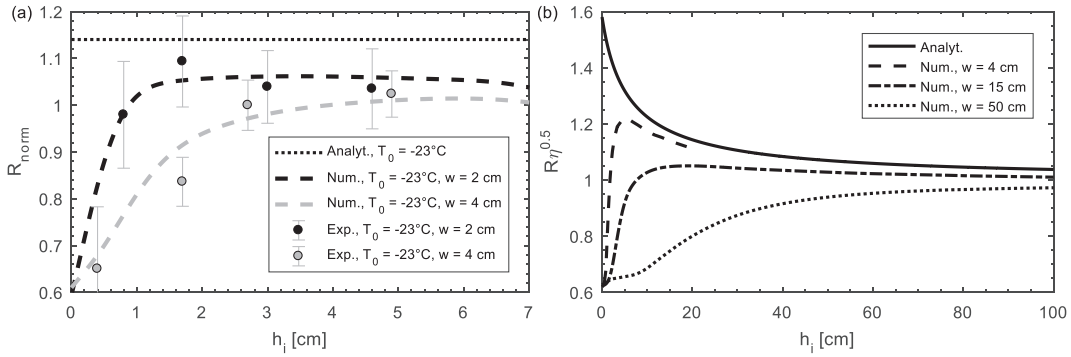

Fig. 10. Values of R_{norm} (a) and $R\eta^{0.5}$ (b) vs the level ice thickness h_i for different block thicknesses w in physical and numerical experiments.

4.2.2. Sail height (surface roughness) and initial block temperature effects

The numerical model confirmed the effect of the initial ice temperature and sail height, with increasing consolidation for increasing sail heights and decreasing initial temperatures (Fig. 11). The effect on R_{norm} values from a decreasing initial temperature of −23 °C was equivalent to the effect from an increasing sail height of 3 cm. The increasing sail height resulting in faster consolidation was due to two factors: the higher sail was due to locally thicker ice and a lower ice surface temperature and corresponding higher conductive heat flux through thin ice (Eqs. (2) and (3)). Additionally, the effective heat transfer coefficient H_{ia} increased due to an increase in the ice surface in comparison to its horizontal projection.

In contrast to our experiments, the sail height of the ice basin and natural ridges mainly depended on the ridge isostatic balance or the balance of gravity and buoyancy forces. Thus, the sail height could not be zero. In our experimental scale, the sail resembled the surface roughness and its impact on heat transfer and the increasing consolidation rate (Fig. 12a). The sail effect and the effect of the initial ice temperature depended on each other and could not be simply added (Fig. 12b).

The effect from large-scale sails in the field also included trapped air or snow volumes. This effect was more complicated and required further investigation. However, we performed additional simulations to investigate the roughness effect for thicker blocks. For simulations with a 15-cm-thick block surface, the roughness had little effect on consolidation, while for 50-cm blocks, a small sail with a height within 1–50 cm resulted in slightly lower ridge consolidation. It corresponded to the field results, as presented by Kharitonov and Morev (2009), showing no effect of a relatively small sail height on the consolidated layer thickness.

4.2.3. Porosity and turbulence effect

The macroporosity is the main parameter defining the difference between a ridge and level ice consolidation, and the effect of both macroporosity and the heat transfer coefficient is considered in R_{norm}. Lower values of the heat transfer coefficient H_{ia} led to a more significant scale effect for similar ice thicknesses (Fig. 3). Only an infinitely high H_{ia} corresponding to Stefan's equation for ice growth led to an immediate equilibrium value of $R{\sim}\eta^{-0.5}$. The numerical model was used to validate Eq. (14) with a constant void thickness w_v, and the varying porosity η_0 was obtained by changing the block size. Fig. 13 shows that both effects were well captured and only slightly overestimated by the analytical model.

The change in porosity in the range from 0.3–0.5 resulted in a 3.5% difference in R_{norm} value, which was smaller than the instrumental errors of the consolidation experiments with a similar scale. However, in the present numerical simulations, an increase in porosity implied a lower block thickness, which in turn increased R_{norm} (see Fig. 10a). Hence, Fig. 13 shows that the block thickness effects could influence the porosity effects and vice versa. The R_{norm} value was almost independent of the heat transfer coefficient H_{ia}. Usage of R_{norm} provided the possibility of comparing the experiments with different porosities and different thickness ranges expecting R_{norm} values approaching a value of 1.

4.2.4. Keel effect

The effect of the limited keel depth k is critical mainly for the experimental setup. In the field, the keel depth to block thickness ratio was often much larger than in our experiments, which resulted in a decreasing trend in R_{norm} towards the end of the experiments, approximately 2 cm before h_c reached the keel bottom (Fig. 11). When the consolidation front was approaching the bottom of the ice blocks, the consolidation rate was decreasing until the front became planar and further consolidation was identical to level ice growth (Fig. 14b). The affected region depended on the scale of the voids between blocks. The numerical modelling results explained the lower R values for the later experimental stages: the solidification rate was slower when the consolidated layer thickness h_c was approaching the values of the keel depth k.

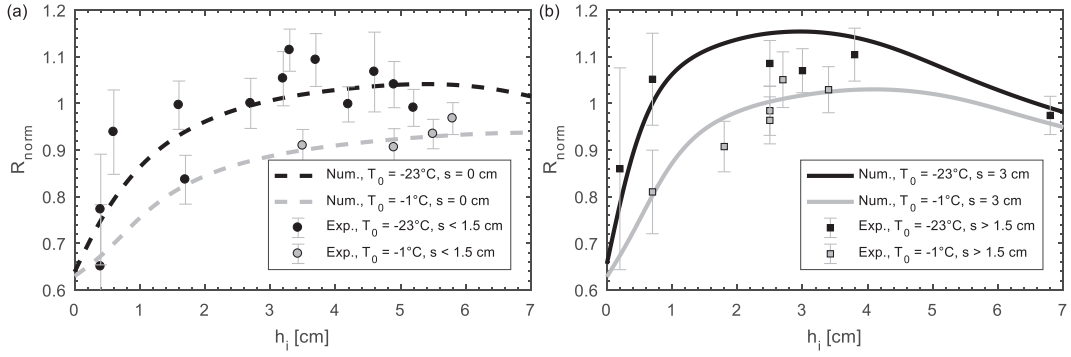

Fig. 11. Temperature effect on the R_{norm} values for experiments with a small (a) and large (b) sail.

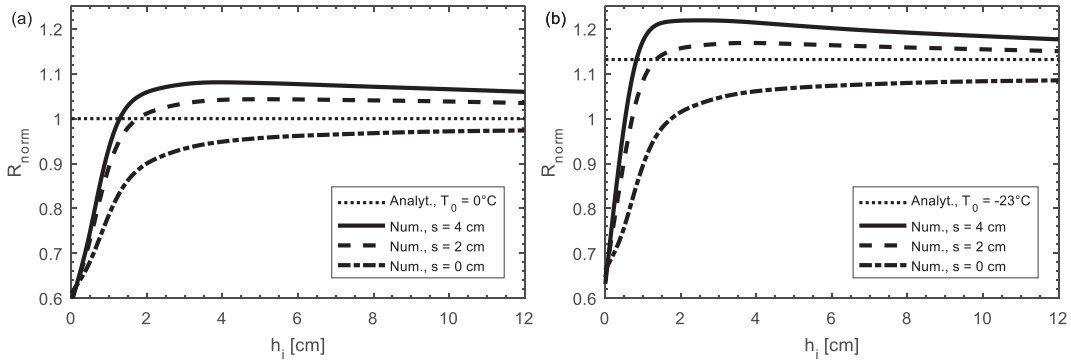

Fig. 12. Values of R_{norm} vs level ice thickness h_i for different sail height s for warm (a) and cold (b) 4-cm-thick ice blocks.

4.2.5. Ice-water interface and temperature distribution

The location of the ice-water interface at different times of the simulation is presented in Fig. 14a. Its shape was changing during the initial phase and when the consolidation front was approaching the ice block bottom. Numerical results for the temperature distribution throughout the experiment are presented in Fig. 14b.

The arch shape of the consolidation front covered the ice volume equivalent to approximately one-quarter of the consolidated layer with a thickness equal to the void width (7 mm for the 2.7-cm voids). The shape usually formed after 1 h of freezing for 4-cm-thick ice blocks. However, it should be noted that in reality, brine released during freezing may lead to different pattern and modes of haline convection, which may influence the porosity evolution due to heat and salt transfer. These convection processes, similar to the details of heat transfer in the atmospheric boundary layer, cannot be addressed herein. However, the size and 2D effects in a pure heat conduction problem can be addressed.

5. Discussion

5.1. Choice of experimental setup

Our experimental setup with a simplified ridge morphology allowed more accurate measurements of macroporosity and consolidated layer thickness in comparison to other methods, and the usage of fresh ice allowed the neglect of complications with composition-dependent thermodynamic variables. The proposed setup also dramatically reduced the preparation time of the experiments, allowing comparisons of the results of solidification with different ridge initial parameters and different scales. The effect of the change in macroporosity within the range of the described experiments was comparable to the effects of other ridge parameters, including the initial block temperature and the sail height. Verification of their effects was only possible using R_{norm}, which allowed the neglect of the effect of macroporosity. Usage of R_{norm} was only possible with high accuracy of the macroporosity measurements, which was provided by the simplified ridge geometry, as described in the experimental setup. As described in Section 1, the effect of ice chemical composition on ice growth was in the range of the ice thickness and ridge porosity measurement errors.

5.2. Comparison across scales

We suggest that the small-scale consolidation process can be divided into several phases. The initial phase starts immediately after ridging, when the level ice and consolidated layer are growing at almost the same rate, and the R value is 1. This phenomenon has also been observed during small-scale fresh ice ridge solidification by Wazney et al. (2019) and during both saline and fresh ice crack refreezing by Petrich et al. (2007). This phase ended when values of R started to approach the value of η^{-1} (Fig. 10b). The initial phase of consolidation can be described only by 2D modelling. The end of this phase usually occurs when the level ice reaches approximately the void width value and R reaches the maximum value. During the following main phase, R was defined by the presented analytical solution described in Section 2. It slowly decreased and approached its equilibrium value of $\eta^{-0.5}$.

The time for consolidation to reach analytical solution values was scale-dependent. It was observed in the large-scale field experiments (Fig. 2b). This definition of the consolidation phases differed from the original definition proposed by Høyland and Liferov (2005). We believe that the duration of the initial phase from that original definition is too small in comparison to the duration of the whole consolidation process and cannot be identified from the thickness development alone.

Analysis of field experiments during consolidation requires knowledge of the ridge macroporosity, the amount of *FDD* before and after ridging, and the thermal insulation provided mostly by snow. These data are usually unavailable, and a level ice growth model is necessary to estimate the ridging time from air temperature data, the ridge block thickness and level ice thickness development. Based on the ridging

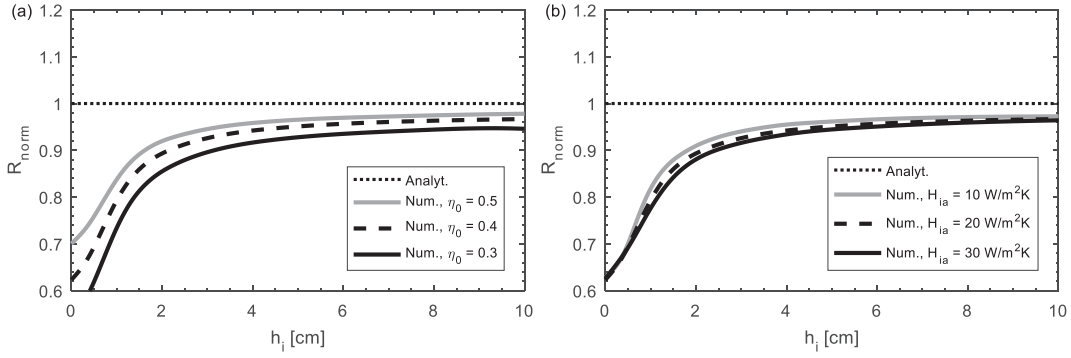

Fig. 13. R_{norm} vs the level ice thickness h_i for different porosities (a) and different heat transfer coefficients H_{ia} (b).

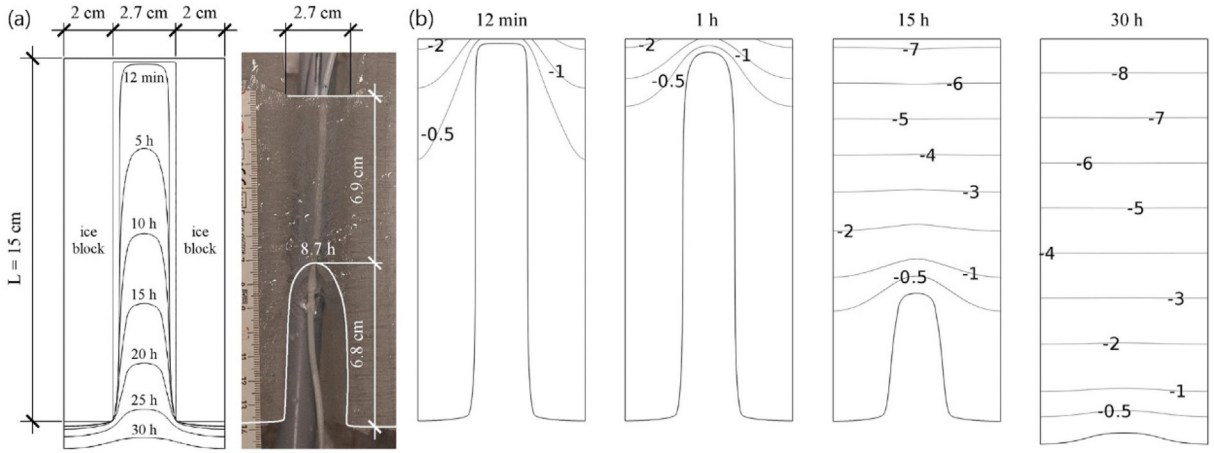

Fig. 14. Ice-water interface from the simulation and after the end of experiment 18 (a) and isotherms from simulations for different stages of the experiment.

time, air temperature, wind speed and snow thickness, the ridge consolidation model can predict its development and provide R values for any experimental time.

One of the differences between the basin and natural ridge consolidation was the presence of level ice around the natural ridge, which decreased the initial R values. The difference between the 1D analytical and 2D numerical solution is presented in Fig. 15. It was assumed that the initial level ice thickness was equal to the thickness of the ice blocks forming the ridge. The level ice initial thickness h_o resulted in changing values of R, and thick blocks caused the season to be too short to reach ${\eta_0}^{-0.5}$.

Application of the described analytical and numerical models for the experiments in different scales and different ice types, including fresh, saline and with dopants, is presented at Fig. 16a. The values of the heat transfer coefficient to simulate these experiments were determined using the level ice growth from the described experiments. The ridge porosity of 0.5 was estimated for the experiments by Timco and Goodrich (1988) from the block length and thickness ratio using the approach of Surkov and Truskov (2003). For the experiment by Blanchet (1998), the ridge porosity was assumed to be equal to the average field value for upper keels of 0.25 according to Pavlov et al. (2016). Both the snow thickness and ridge macroporosity were measured in experiments by Høyland (2002).

Both analytical and numerical models provided very accurate predictions of consolidation development. For the small-scale tests by Timco and Goodrich (1988), most of the key parameters for consolidation were unknown, including the ridge porosity, initial block temperature and surface roughness. The faster decrease in the consolidation rate observed in experiments by Timco and Goodrich (1988) in comparison to our analytical solution could be due to the surface roughness effect described in this paper and their increases with depth macroporosity values measured in the field by Pavlov et al. (2016). The similarity of the results from our experiments and those of Timco and Goodrich (1988) confirms that our experimental setup is applicable for the small-scale consolidation problem (Fig. 16b).

The final problem concerns how to compare the results of field and laboratory experiments. In general, they have different scales, different dominating heat exchange mechanisms (turbulence for smaller scales and radiation for larger scales), and different porosities, making the normalisation necessary for comparison very complicated. The R value differs for differences in wind speed, top surface insulation, and porosity and is scale-dependant for both the final thickness and the initial block thickness. The results could be reanalysed using the presented model and result in divergence from its predictions. Simultaneously, non-critical factors might be excluded from the comparison to generate a smaller experimental matrix and allow comparisons of a larger amount of field data.

5.3. Choice of boundary conditions

The analytical model is one-dimensional and cannot directly include effects from the sail. The two-dimensional numerical model is based on

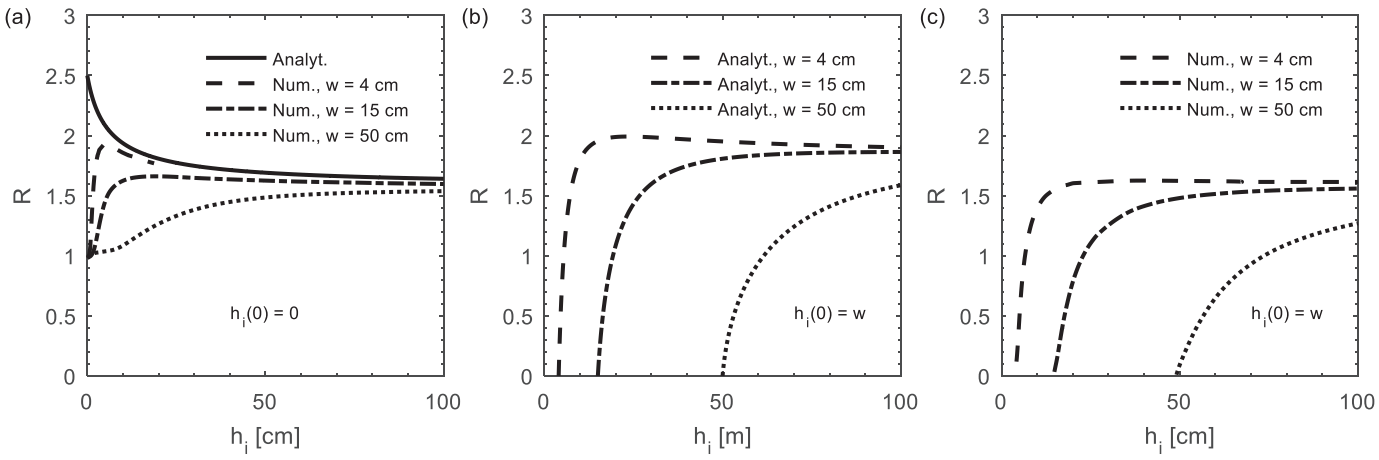

Fig. 15. R vs level ice thickness h_i for 4, 15 and 50-cm-wide blocks and a porosity of 0.4 with a 0 initial level ice thickness (a) and a ridge block initial level ice thickness from analytical solution (b) and from numerical simulations (c).

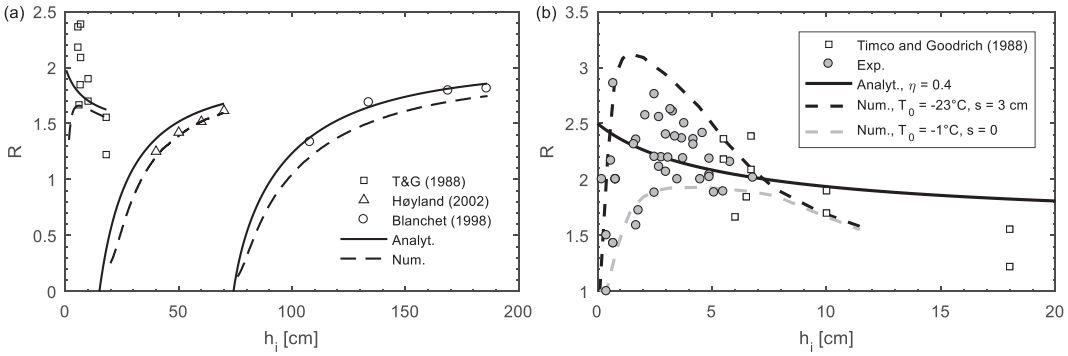

Fig. 16. Comparison of R values from experiments by Timco and Goodrich (1988), Blanchet (1998), and Høyland (2002) and from analytical and numerical solutions for initial experimental conditions for large scales (a) and small scales (b).

several assumptions, including equal values of heat transfer coefficient for the ridge and level ice top surface. It accurately describes the experimental consolidated layer growth dependence on the sail height, meaning that the same convectional heat transfer coefficient can be used for both level ice and small-scale ridge models. Using our numerical model, it was possible to use realistic ridge cross-sections with extended surfaces representing the ridge sail. For the presented level ice growth, the experiment convectional heat transfer coefficient showed significant variation with the value of 19 $\pm$ 2 W/m^{2}K based on the measured temperature profile. The heat transfer coefficient values for the ridges with small sails were in the same range as those for level ice but significantly higher than those for larger sail heights (Fig. 8b). Based on the experiments with different initial block temperatures, we can conclude that most of the sensible heat was converted into latent heat and changed the porosity after ridge formation. Considering only parameters such as the initial block temperature, macroporosity, and sail height was it possible to confirm the experimental ice growth results with numerical results (Fig. 11).

Both analytical and numerical models were able to predict consolidation rates for experiments with different scales and ice types (Fig. 16). We also showed the potential reason for consolidated layer thickness overestimation using vertical temperature profiles (Fig. 14b): ice blocks could be significantly colder than the water freezing temperature even below the minimum thickness of the consolidated layer. The relative error values could be much higher for the initial stages of the experiment, which led to the suggestion that more detailed and advanced algorithms should be described and implemented to determine the consolidated layer thickness from the temperature profiles.

6. Summary and conclusions

This paper contributes to a better understanding of ridge solidification and scale effects. Data from previous experiments on different scales were analysed, and a possible explanation of ridge consolidated layer development was described. Twenty laboratory experiments were performed to improve our understanding of factors governing consolidation of small-scale ridges. The main findings of the recent study are summarized as follows:

- The analytical model of ice ridge solidification, which is able to explain observed scale effects on consolidated layer growth, is presented. It allows the comparison of experiments for ridges with different porosities, ice block initial temperatures, subjected to air with different convectional heat transfer coefficients using the introduced normalisation factor R_{norm}. The ratio of the consolidated layer and surrounding level ice thickness based on that solution mainly depended on the ridge macroporosity η, starting at the value of η^{-1} and approaching $\eta^{-0.5}$ for thick ice.
- The new configuration of laboratory experiments in ridge consolidation was described to improve the accuracy of the main parameters governing that process. In the provided experiments, the consolidated layer reached a thickness up to 2.2–2.8 times greater than level ice for the ridge macroporosity η of 0.4, similar to the described analytical model predictions of η^{-1}.
- A numerical model, which was able to predict effects on the consolidation rates from sail height, block thickness, block initial temperature and macroporosity, was described and validated using the provided experiments. The sail height had a significant effect on the small-scale consolidation, leading to up to a 40% thicker consolidated layer for the sail height of 3 cm compared to the level area. This phenomenon was observed in both experiments and numerical simulations, and it contrasts with typical observations for large-scale ridges.
- Both experiments and numerical simulations confirmed that the consolidated layer thickness was initially growing slower than predicted by the analytical solution. The analytical solution was approached when the thickness of ice growing in voids reached the thickness of the ridge blocks.

Acknowledgements

The authors wish to acknowledge the support of the Research Council of Norway through the Centre of Research based Innovation SAMCoT grant 203471 (Sustainable Arctic Marine and Coastal Technology), the RCN PETROMAKS2 grant 243812 (Microscale Interaction of Oil with Sea Ice for Detection and Environmental Risk Management in Sustainable Operations, MOSIDEO), as well as the support of all the SAMCoT partners.

References

Adams, C.M., French, D.N., Kingery, W.D., 1960. Solidification of sea ice. J. Glaciol. 3 (28), 745–760. https://doi.org/10.3189/S0022143000018050.

Alexiades, V., Hannoun, N., Mai, T., 2003. Tin melting: effect of grid size and scheme on the numerical solution. In: Fifth Mississippi State Conference on Differential Equations and Computational Simulations, pp. 55–69. ftp://ftp.zcu.cz/pub/doc/EJDE/conf-proc/10/a5/alexiades.pdf.

Ashton, G.D., 1989. Thin ice growth. Water Resour. Res. 25 (3), 564–566. https://doi.org/10.1029/WR025i003p00564.

Blanchet, D., 1998. Ice loads from first-year ice ridges and rubble fields. Can. J. Civ. Eng. 25 (2), 206–219. https://doi.org/10.1139/l97-073.

Bonath, V., Petrich, C., Sand, B., Fransson, L., Cwirzen, A., 2018. Morphology, internal structure and formation of ice ridges in the sea around Svalbard. Cold Reg. Sci. Technol. 155, 263–279. https://doi.org/10.1016/j.coldregions.2018.08.011.

Feistel, R., Hagen, E., 1998. A Gibbs thermodynamic potential of sea ice. Cold Reg. Sci. Technol. 28 (2), 83–142. https://doi.org/10.1016/S0165-232X(98)00014-7.

Griewank, P.J., Notz, D., 2013. Insights into brine dynamics and sea ice desalination from a 1-D model study of gravity drainage. J. Geophys. Res. Oceans 118 (7), 3370–3386. https://doi.org/10.1002/jgrc.20247.

Høyland, K.V., 2002. Consolidation of first-year sea ice ridges. J. Geophys. Res. 107 (C6). https://doi.org/10.1029/2000jc000526.

Høyland, K.V., 2007. Morphology and small-scale strength of ridges in the North-western Barents Sea. Cold Reg. Sci. Technol. 48 (3), 169–187. https://doi.org/10.1016/j.

coldregions.2007.01.006.
Høyland, K.V., 2010. Thermal aspects of model basin ridges, Proc. of 20th Ice Symposium (IAHR). Lahti, Finland. http://riverice.civil.ualberta.ca/IAHR%20Proc/20th%20Ice%20Symp%20Lahti%202010/Papers/066_Hoyland.pdf.
Høyland, K.V., Liferov, P., 2005. On the initial phase of consolidation. Cold Reg. Sci. Technol. 41 (1), 49–59. https://doi.org/10.1016/j.coldregions.2004.09.003.
ISO 19906, 2010. Petroleum and natural gas industries – arctic offshore structures. Int. Stand. 2010 (50). https://doi.org/10.5594/J09750.
Kharitonov, V.V., 2008. Internal structure of ice ridges and stamukhas based on thermal drilling data. Cold Reg. Sci. Technol. 52 (3), 302–325. https://doi.org/10.1016/j.coldregions.2007.04.020.
Kharitonov, V.V., Morev, V.A., 2009. Hummocks near the North Pole 25 drifting station (in Russian). Meteorol. Gidrol. 2009 (6), 68–73.
Langhaar, H., 1951. Dimensional Analysis and Theory of Models. John Wiley and Sons 166 p.
Leppäranta, M., 1993. A review of analytical models of sea-ice growth. Atmosphere-Ocean 31 (1), 123–138. https://doi.org/10.1080/07055900.1993.9649465.
Leppäranta, M., Hakala, R., 1992. The structure and strength of first-year ice ridges in the Baltic Sea. Cold Reg. Sci. Technol. 20 (3), 295–311. https://doi.org/10.1016/0165-232X(92)90036-T.
Leppäranta, M., Lensu, M., Kosloff, P., Veitch, B., 1995. The life story of a first-year sea ice ridge. Cold Reg. Sci. Technol. 23 (3), 279–290. https://doi.org/10.1016/0165-232X(94)00019-T.
Liu, Y.C., Chao, L.S., 2006. Modified effective specific heat method of solidification problems. Mater. Trans. 47 (11), 2737–2744. https://doi.org/10.2320/matertrans.47.2737.
Maykut, G.A., Untersteiner, N., 1969. Numerical Prediction of the Thermodynamic Response of Arctic Sea Ice to Environment Changes. The Rand Corporation, Santa Monica, California RM-6093-PR. https://www.rand.org/pubs/research_memoranda/RM6093.html.
Maykut, G.A., Untersteiner, N., 1971. Some results from a time–dependent, thermodynamic model of sea ice. J. Geophys. Res. 76, 1550–1575.
Millero, F.J., 2010. History of the equation of state of seawater. Oceanography 23 (3), 18–33. https://doi.org/10.5670/oceanog.2010.21.
Notz, D., 2005. Thermodynamic and Fluid-Dynamical Processes in Sea Ice. University of Cambridge. http://mpimet.mpg.de/fileadmin/staff/notzdirk/Notz_PhD_abstract.pdf.
Palmer, A., Dempsey, J., 2009. Model tests in ice. In: Port and Ocean Engineering Under Arctic Conditions Conference (POAC 09), Lulea, Sweden, 1–10, POAC09-40. http://www.poac.com/Papers/POAC09_01-71.zip.
Pavlov, V.A., Kornishin, K.A., Efimov, Y.O., Mironov, E.U., Guzenko, R.B., Kharitonov, V.V., 2016. Peculiarities of consolidated layer growth of the Kara and Laptev Sea ice ridges. Neftyanoe Khozyaystvo – Oil Ind. 11, 49–54.
Petrich, C., Langhorne, P.J., Haskell, T.G., 2007. Formation and structure of refrozen cracks in land-fast first-year sea ice. J. Geophys. Res. Oceans 112 (4). https://doi.org/10.1029/2006JC003466.
Pounder, E.R., 1965. The Physics of Ice. Pergamon Press, Oxford, UK. https://doi.org/10.3189/S0022143000019353.
Repetto-Llamazares, A., 2010. Review in model basin ridges. In: Proc. of the 20th Ice Symposium (IAHR), Lahti, Finland.
Schwerdtfeger, P., 1963. The thermal properties of sea ice. J. Glaciol. 789–807. https://doi.org/10.3189/S0022143000028379.
Stefan, J., 1891. Ueber die Theorie der Eisbildung, insbesondere über die Eisbildung im Polarmeere. Ann. Phys. 278 (2), 269–286. https://doi.org/10.1002/andp.18912780206.
Strub-Klein, L., Høyland, K.V., 2011. One season of a 1st year sea ice ridge investigation – Winter 2009. In: Proceedings of 21th International Conference on Port and Ocean under Arctic Conditions (POAC) Montreal, Canada.
Strub-Klein, L., Sudom, D., 2012. A comprehensive analysis of the morphology of first-year sea ice ridges. Cold Reg. Sci. Technol. 82, 94–109. https://doi.org/10.1016/j.coldregions.2012.05.014.
Surkov, G.A., Truskov, P.A., 2003. Parameters of hummock-forming blocks of ice. In: Proceedings of the 17th International Conference on Port and Ocean Engineering under Arctic Conditions (POAC) 2003. Trondheim, Norway. 2. pp. 87–102. http://www.poac.com/Papers/POAC03_V2.zip.
Timco, G.W., Goodrich, L.E., 1988. Ice rubble consolidation. In: Proceedings of 9th International Symposium on Ice, International Association of Hydraulic Engineering. 1. pp. 537–548.
Wazney, L., Clark, S.P., Malenchak, J., 2019. Laboratory investigation of the consolidation resistance of a rubble river ice cover with a thermally grown solid crust. Cold Reg. Sci. Technol. 157, 86–96. https://doi.org/10.1016/j.coldregions.2018.10.001.
Weast, R.C., 1971. Handbook of Chemistry and Physics, 52 edition. Chemical Rubber Co., Cleveland, OH.
World Meteorological Organization, 1970. WMO Sea Ice Nomenclature (supplement No 5.1989). Technical Report MO No. 259.TP.145. World Meteorological Organization, Geneva, Switzerland.
Yen, Y.C., 1981. Review of Thermal Properties of Snow, Ice, and Sea Ice. CRREL Res. Rept. 81-10, U.S. Army Cold Reg. Res. and Eng. Lab., Hanover, NH, US.
Yen, Y.C., Cheng, K.C., Fukusako, S., 1991. Review of intrinsic thermophysical properties of snow, ice, sea ice, and frost. In: Zarling, J.P., Faussett, S.L. (Eds.), Proceedings 3rd International Symposium on Cold Regions Heat Transfer, Fairbanks, AK, June 11–14, 1991. University of Alaska, Fairbanks, US, pp. 187–218.